A band structure analysis of the coexistence of superconductivity and magnetism in $(Ho,Dy)Ni_2B_2C$

2006 J. Phys.: Condens. Matter 18 5973

(http://iopscience.iop.org/0953-8984/18/26/016)

INSTITUTE OF PHYSICS PUBLISHING JOURNAL OF PHYSICS: CONDENSED MATTER

J. Phys.: Condens. Matter **18** (2006) 5973–5983 doi:10.1088/0953-8984/18/26/016

A band structure analysis of the coexistence of superconductivity and magnetism in (Ho, Dy)Ni_2B_2C

A O Shorikov[1], **V I Anisimov**[1] **and M Sigrist**[2]

[1] Institute of Metal Physics, Russian Academy of Sciences, 620041 Yekaterinburg GSP-170, Russia
[2] Theoretische Physik, ETH-Zürich, CH-8093 Zürich, Switzerland

Received 20 April 2006
Published 19 June 2006
Online at stacks.iop.org/JPhysCM/18/5973

Abstract

The phenomenological theory of complex interplay of superconductivity and magnetism in $Ho_{1-x}Dy_xNi_2B_2C$ by Doh *et al* (1999 *Phys. Rev. Lett.* **83** 5350) is based on the multi-band picture with at least one band which is strongly dominated by Ni 3d-electron orbitals. These orbitals are insensitive to the antiferromagnetic order of the (Ho, Dy) 4f-electrons, found in these alloys. In the present study we show by detailed analysis of the band structure that indeed such a band can be identified. This provides a microscopic justification of the basic idea underlying the phenomenological discussion.

(Some figures in this article are in colour only in the electronic version)

1. Introduction

The discovery of the nickel–boron-carbide compounds RNi_2B_2C roughly a decade ago has reinitiated the study of magnetic superconductivity, as these systems turn out to exhibit various remarkable properties [2–6]. In the absence of magnetism these compounds are superconductors with a rather high transition temperature T_c of about 16.5 K. For the rare earth atom we may choose freely in the row of the periodic table between Lu and Gd (R = Lu, Tm, Er, Ho, Dy, Tb, Gd). The partially filled 4f-shells of R form localized magnetic moments of varying magnitudes J which induce magnetic order at low enough temperature. The sizable spin–orbit coupling is responsible for the different ordering patterns [7]. The view that RKKY-interaction mediates the order is corroborated by the observation that the transition temperature T_N roughly scales with the de Gennes factor $dG = (g_J - 1)^2 J(J + 1)$ (g_J: the gyromagnetic ratio) [6, 8]. Thus the magnetism is modified by the choice of R. Naturally the magnetism interferes with superconductivity. The tunability of the magnetism is a lucky coincidence allowing for the study of the interplay between the local-moment magnetism and superconductivity under varying conditions. For some compounds the onset of magnetism lies at higher temperature than for the superconductivity, and for others the opposite holds [6]. Despite the presence

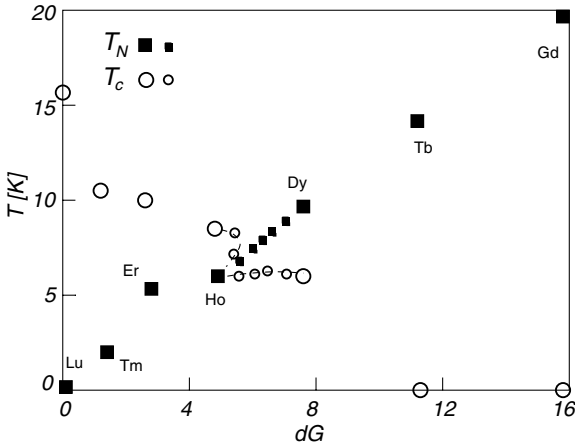

Figure 1. Phase diagram: T_c and T_N versus de Gennes factor for nickel–boron-carbide series following [6].

of magnetism the superconducting phase is most likely due to electron–phonon coupling with basically s-wave spin singlet symmetry [6] (for a review see also [9]).

It is well-known that the influence of magnetic moments and their order is detrimental to the superconducting state. First of all magnetic impurities are pair breaking scatterers in conventional superconductors and suppress the critical temperature, roughly proportional to dG times the impurity concentration. The situation is more complex when the magnetic moments are positioned regularly, and if they form an ordered state in addition. Still one expects that the coupling to the conduction electrons should be roughly governed by the de Gennes factor dG. Considering the sequence of RNi_2B_2C we observe indeed an essentially linear increase of T_N with growing dG. Simultaneously T_c decreases apparently in a monotonic way. However, things turn out to be more subtle, as we will discuss shortly [8].

Beginning with the contrasts of the extreme members of this class, we find that the non-magnetic Lu and Yb display superconductivity below $T_c = 15.5$ or 16.5 K, respectively. These materials have recently been studied intensively, because of their very anisotropic s-wave pairing gap which makes their low-energy properties rather sensitive to the influence of non-magnetic impurities [10–13, 9]. Turning to R = Tb and Gd, magnetic order is found below $T_N = 16$ and 19 K, respectively, due to their large magnetic moments. The magnetism in these compounds suppresses superconductivity entirely. For intermediate de Gennes factors, however, superconductivity and magnetism coexist. The magnetism is rather robust and essentially unaffected by the presence of superconductivity, while superconductivity is visibly influenced by the appearance of magnetic order as well as magnetic fluctuations.

A highly intriguing and unexpected behaviour has been reported for the intermediate compounds $HoNi_2B_2C$ and $DyNi_2B_2C$. Their magnetic and superconducting onset temperatures are reversed, i.e. for Ho $T_c > T_N$ while Dy $T_c < T_N$. The coincidence that the magnetic orders of the two compounds are identical apart from the size of the moments provides the opportunity to study the crossing of T_c and T_N by doping: $Ho_{1-x}Dy_xNi_2B_2C$, where the 'continuous' variation of x is linked with a 'continuous' change of the average localized magnetic moment J and, thus, the de Gennes factor dG. The Néel temperature T_N indeed follows very well the simple relation $T_N \propto dG$, giving a simple linear interpolation between the T_N-values of the two pure compounds. However, for the superconducting transition temperature one observes a rather anomalous x-dependence (figure 1). This feature has been

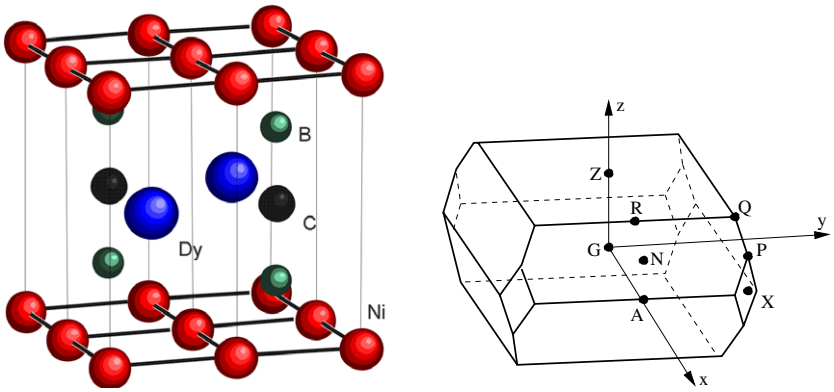

Figure 2. Crystal structure of $DyNi_2B_2C$ (left panel) and the corresponding Brillouin zone (right panel).

advertised as the violation of de Gennes scaling ($\Delta T_c \propto dG$). A first unusual aspect is the reentrant behaviour of normal phase for small x around $T \approx T_N$. The superconducting phase (with $T_c > T_N$) seems to be weakened close to T_N and, against intuition, recovers again as the magnetic order is established. A second extraordinary property is the basically x-independent T_c for $0.3 < x \leqslant 1$ in the magnetically ordered phase ($T_c < T_N$) (see figure 1). The reentrant behaviour has been attributed by Doh *et al* [1] to the influence of magnetic fluctuations close to the ordering temperature. The constant T_c, moreover, has been explained by assuming that superconductivity involves several bands, which are coupled to the magnetic order in different ways [1]. This argument is based on the assumption that the Ni 3d-orbitals remain unaffected by the magnetic order on the Ho-/Dy-ions, due to the cancelling of the four moments nearest to each Ni-site (geometric aspect). The structure of the magnetic order shows in-plane ferromagnetic alignment for each Dy-layer but staggering between the layers. The nearest-neighbour Dy-sites above and below each Ni have opposite moment, leading to a vanishing net moment on the Ni-site. For this type of model a rather thorough understanding of the phase diagram of $Ho_{1-x}Dy_xNi_2B_2C$ has been achieved on a phenomenological basis [1, 14]. In order to work properly, this multi-band model requires, however, that there is at least one band which is almost exclusively dominated by the Ni 3d-orbitals at the Fermi surface. The present study is devoted to the detailed analysis of the LDA-band structure of $DyNi_2B_2C$ in order to identify the relevant bands as the essential ingredient of the phenomenological theory.

2. Band structure calculation

The $HoNi_2B_2C$ and $DyNi_2B_2C$ compounds have the same crystal structure and the same form of spin ordering. Thus we will restrict our calculations to the case of $DyNi_2B_2C$. The effect of substitution of dysprosium by holmium may be taken into account by decreasing the value of total magnetic moment. $DyNi_2B_2C$ crystallizes in a tetragonal body-centred structure with lattice parameters $a = 3.5342$ Å and $c = 10.4878$ Å [15]. The Ni ions form square lattice layers parallel to the ab-plane (see figure 2 left panel) and are coupled via B–C–B complexes with Dy ions lying between the layers. These B–C–B complexes and Dy ions are situated above the centres of the plaquettes formed by the Ni lattice and alternate with each other.

The 4f-states of the rare earth atoms are well localized. The analysis of x-ray and photoemission spectra shows that occupied and empty 4f-bands are situated 3–5 eV below and above Fermi energy [16]. In contrast, results of the density functional theory show the

appearance of a partially filled f-band on the Fermi level [17, 18]. There are two ways to deal with this deficiency. One way is to treat the f-states as pseudocore states, and the other way is to include Coulomb interaction corrections by means of the LDA + U method to split the energies of occupied and empty f-bands. The first case is appropriate if f-states did not affect the physics of the problem at all. The second one allows us to take into account the interaction of f-states with the itinerant bands. Because we are interested in the influence of the magnetic ordering of 4f-electrons on the states near the Fermi energy responsible for superconductivity, we use the LDA + U method to treat the 4f-states of the rare earth element.

The band structure of $DyNi_2B_2C$ was calculated using the LDA + U method [19] in the TB-LMTO-ASA (tight-binding linear-muffin-tin-orbitals atomic-sphere-approximation) computation scheme [20, 21]. On-site Coulomb repulsion and Stoner exchange parameters for the f-shell of Dy have been calculated using the constrained LDA procedure [22, 23] and were determined as 11 and 0.9 eV respectively. Other states, apart from the Dy 4f-states, were considered as itinerant and the LDA + U potential correction was not applied to those. The resulting bands presented below were plotted using the Brillouin zone of the body-centred tetragonal lattice of $DyNi_2B_2C$ (it is shown in figure 2 (right panel) together with symmetry points notation).

The main goal of our calculations is to determine the origin of the bands crossing the Fermi level and to examine whether they are strongly affected by the ordering of the magnetic moment of the rare earth ions. To this end we performed two sets of band structure calculations with different magnetic ordering. One is the antiferromagnetic ordering (AFM) realized in the physical system, the other is a completely ferromagnetic order (FM). The bands calculated for the FM case were averaged for the two spin directions in order to obtain an approximation for paramagnetic case above the Néel temperature. The comparison of bands in the case of AFM ordering with the 'paramagnetic' bands shows the influence of the spin ordering below the Néel temperature on the electronic structure. To treat AFM ordering the unit cell of $DyNi_2B_2C$ has to be doubled and the body-centred tetragonal lattice has to be converted into a primitive tetragonal one. The calculations for FM order were done with the same doubled unit cell for comparison. However, for the eventual analysis it is more convenient to view the bands along the high-symmetry directions in the Brillouin zone of the body-centred tetragonal lattice (figure 2 right panel).

We have found a relatively strong splitting of the bands crossing the Fermi level in the PN-direction (see inset B in figure 3), while another set of bands with Fermi surfaces in the G–X direction shows a negligible effect from AFM order (see inset A in figure 3). The model proposed in [1] requires the existence of two types of band crossing the Fermi levels with strongly different coupling to the magnetic order. In order to understand why different bands (insets A and B) react differently on the Dy-spin ordering we have performed an orbital contribution analysis. We are here mainly interested in the contribution of Ni 3d-orbitals, since due to the symmetry the Ni-orbitals should be insensitive to the spin ordering, and 2p-states of boron and carbon which are exposed to the influence of the Dy magnetic moments.

In figure 4, the bands with strong contributions form 2p-states of the B_2C complex (left panel) and from Ni 3d-states (right panel) are presented. The thickness of the band on the figures is proportional to the contribution of the corresponding state. The results for Ni 3d-orbitals of $d_{3z^2-r^2}$, d_{xy}, $d_{x^2-y^2}$ symmetry are shown separately in figures 5 and 6.

3. Band structure analysis

We now turn to identification of the Fermi surfaces which are least affected by the Dy magnetic moments in the ordered phase. For this purpose a qualitative analysis of the band structure

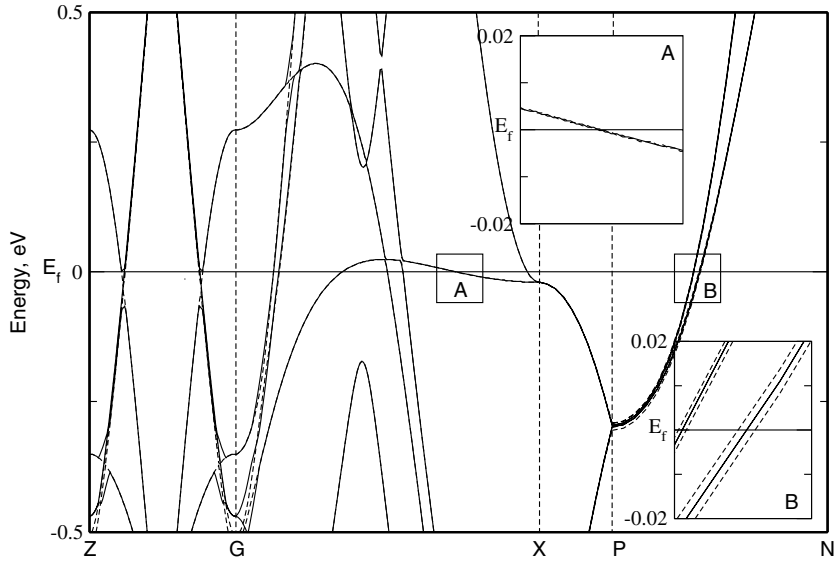

Figure 3. Influence of magnetism on the bands of $DyNi_2B_2C$. Dashed lines correspond to the bands calculated for the AFM-order of the Dy moments. The solid lines correspond to the paramagnetic bands. Two typical Fermi surface crossings are enlarged in the insets, showing that the effect of magnetism is strong for the bands crossing the Fermi level in the PN direction (inset B), but weak for the direction GX (inset A).

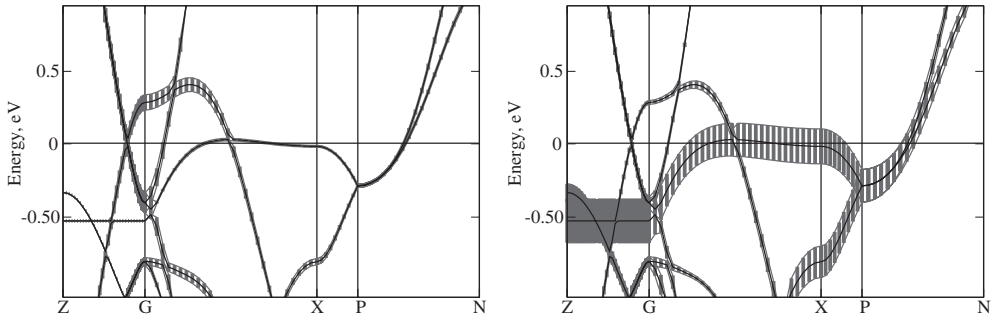

Figure 4. The partial contributions of 2p-orbitals of the B_2C-cluster (left panel) and the Ni 3d-orbtals to different bands of $DyNi_2B_2C$ obtained in non-magnetic calculations. The weights are proportional to the thickness of bands.

based on the most dominant orbitals involved in the band structure at the Fermi level will give some useful insight. As mentioned above, the bands at the Fermi energy consist almost exclusively of the B and C 2p-orbitals and the Ni 3d-orbitals. The Dy-orbitals play a minor role in the metallicity of this compound. It is important to notice that the B and C 2p-electrons act as a bridge in the transfer of the magnetic moment from the localized 4f-orbitals of the Dy-ions to the conduction electrons, which occurs mainly through the hybridization with the Dy 5d-orbitals that are spin-polarized by the presence of magnetic moment on 4f-electrons. Thus the content of the B and C 2p-electrons in the bands crossing the Fermi level is crucial to our analysis.

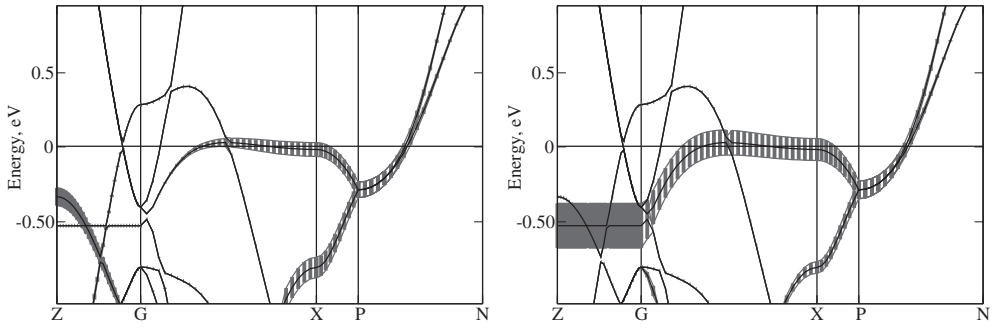

Figure 5. Partial contributions of the Ni $3d_{3z^2-1}$-orbitals (left panel) and Ni $3d_{xy}$-orbitals (right panel). The weights are proportional to the thickness of bands.

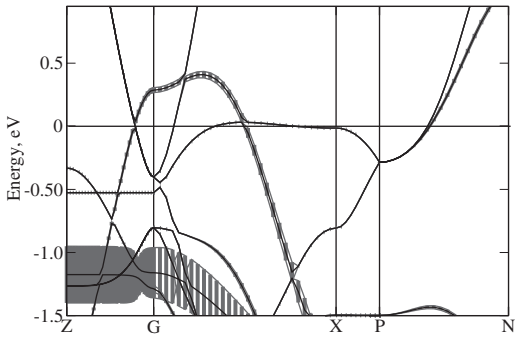

Figure 6. Partial contributions of Ni $d_{x^2-y^2}$-orbitals. The weight is proportional to the thickness of bands.

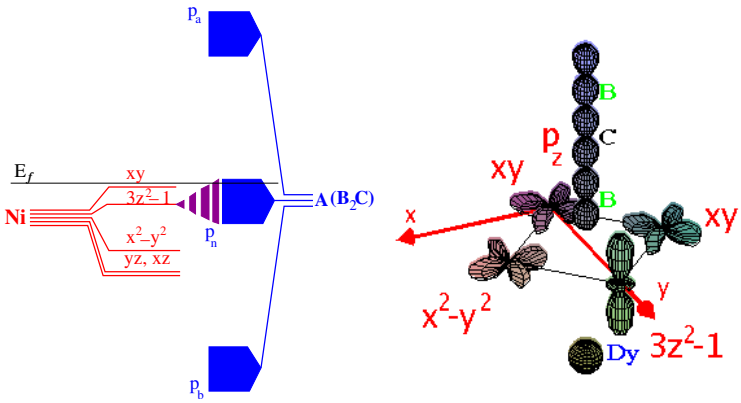

Figure 7. Model scheme of the electronic states (left panel) and mutual orientation of B_2C p-orbitals and Ni d-orbitals (right panel) in $DyNi_2B_2C$.

For our analysis it is useful to distinguish several subgroups of the relevant atomic orbitals. We start with the subunit $A = B_2C$ which appears as a chain B–C–B and whose partially filled 2p-orbitals form energetically well-separated bonding, non-bonding and antibonding combinations (see figure 7 left panel). It is the non-bonding combination that is relevant for

Table 1. Nearest-neighbour hybridization matrix elements for the Ni 3d- and A 2p-orbitals. $sx = \sin(k_x a/2)$, $sy = \sin(k_y a/2)$, $c = \cos(k_x a) - \cos(k_y a)$, $g_{1\pm} = \{\cos^2(k_x a/2) + \cos^2(k_y a/2) \pm 2\cos(k_z c/2)\cos(k_x a/2)\cos(k_y a/2)\}^{1/2}$, and a and c are the unit cell lattice constants in the basal plane and along the z-axis, respectively.

	d_{xy}	$d_{3z^2-r^2}$	$d_{x^2-y^2}$	$p_{x,y}$	p_z
d_{xy}	—	$sx\ sy$	—	—	—
$d_{3z^2-r^2}$	$sx\ sy$	—	c	$sx,\ sy$	g_{1-}
$d_{x^2-y^2}$	—	c	—	$sx,\ sy$	g_{1+}
$p_{x,y}$	—	$sx,\ sy$	$sx,\ sy$	—	—
p_z	—	g_{1-}	g_{1+}	—	—

the bands at the Fermi energy. The p_z-like orbital lies energetically lower than the degenerate $p_{x,y}$-like orbitals. The A-units form together with Dy-ions the layers that alternate with the Ni-layer. Their position lies above the centres of plaquettes in Ni-square lattice so that the Dy and A alternate in chequerboard fashion.

The Ni 3d-orbitals can be separated into three groups forming different bands in Ni_2A-units. The band structure data suggest distinguishing the subsets ($d_{3z^2-r^2}$, d_{xy}), ($d_{x^2-y^2}$) and (d_{zx}, d_{yz}) (see figure 7 left panel). These subsets are not entirely independent, but have very different pattern of hybridization with the A 2p-orbitals.

The set (I) ($d_{3z^2-r^2}$, d_{xy}) of the Ni 3d-orbitals yields two important bands (see figure 5). The in-plane dispersion is dominated mainly by their direct ddσ-hybridization along the [110] and [1$\bar{1}$0] directions. The z-axis dispersion involves mainly the A $p_{x,y}$-orbitals hybridizing with Ni $d_{3z^2-r^2}$-orbitals and to a lesser extent the p_z-orbitals. The orbital symmetry (in particular, the odd-parity of $p_{x,y}$ under in-plane inversion, $(x, y, z) \rightarrow (-x, -y, z)$) suggest that the bands close to the G- and X-points are dominantly of Ni 3d character, as we will see more clearly below. The second subsystem (II) containing only the $d_{x^2-y^2}$-orbital also contributes bands to the Fermi level (see figure 6). In this case all A 2p-orbitals hybridize strongly, in particular, the p_z-orbital (see figure 7 right panel), and the hybridization is strong at the G-point. Finally, the subset (III) involving (d_{zx}, d_{yz}) is unimportant, since these orbitals remain at lower energy due to the crystal field splitting (see figure 7 left panel). However for all orbitals belonging to subset (I) and (II) no pure pdσ- or pdπ-bond is realized. Following Slater–Koster [24] we can express the hybridization in terms of two-centre integrals (pdσ, pdπ) for d_{3z^2-1}- and p_z-orbitals (0.32, 0.32) d_{3z^2-1}- and p_y-orbitals (0.21, 0.48). The hybridization of $d_{x^2-y^2}$- with p_z-orbitals is weak (0.16, 0.19) as well as with p_y- or p_x-orbitals (0.11, 0.38).

In the following we will characterize the Fermi surfaces in terms of the subsets (I) and (II). We gain also further insight by analysing the important hybridizations between different orbitals.

3.1. Hybridization of different orbitals

The large number of orbitals and bands prevents us from providing a reasonably simple effective tight-binding model which would fit the LDA band structure. Thus we concentrate here on a qualitative account of the hybridization of the different orbitals among each other within the Brillouin zone, which yields the most instructive information for our purpose.

The expressions for the nearest-neighbour hybridization matrix elements between different orbitals are given in table 1. For their calculation we have to take into account that the unit cell has the formula unit Ni_2A, i.e. involves two Ni-units and one A-unit. The hybridization of the d_{xy}-orbital of subset (I) with the A p-orbitals is neglected in table 1, since d_{xy} is concentrated

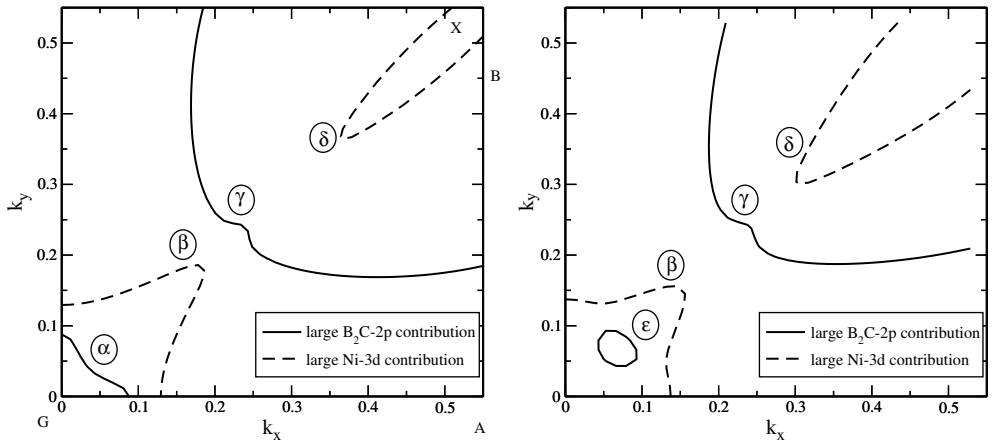

Figure 8. Cuts through the Brillouin zone perpendicular to [001] at $k_z = 0$ (left panel) and $k_z = 0.8$ (right panel). Fermi surfaces dominated by Ni d-orbitals are depicted with dashed lines and the ones with strong (B–C–B)-p character are drawn by solid lines.

in the basal plane and has little overlap with the A-unit which lies roughly $\pm c/2$ out of plane. Moreover, from the symmetry point of view there can be no hybridization with the A p_z-orbital, and with the $p_{x,y}$-orbitals only $pd\pi$-hybridization is possible. Also with the $d_{x^2-y^2}$-orbital of the subset (II) there is no nearest-neighbour overlap by symmetry. The only hybridization is realized with the $d_{3z^2-r^2}$-orbital, also in subset (I), which vanishes as one approaches the G-point. For the $d_{3z^2-r^2}$-orbital the hybridization is expected with all p-orbitals of the A-units as well as with $d_{x^2-y^2}$, besides d_{xz}. Also here the hybridization is cancelled at the G-point and becomes larger towards the Brillouin zone boundary. Except for the hybridization with p_z all are strongly dependent on the direction of $\boldsymbol{k}$. Finally, the $d_{x^2-y^2}$-orbital has a stronger overlap with the 2p-orbitals and couples particularly strongly to the p_z-orbital around the G-point.

3.2. Important Fermi surfaces

In figure 8–10 we show a set of cuts through the Brillouin zone, displaying the important Fermi surfaces. We distinguish five basic sheets. Closest to the G-point is an electron-like Fermi surface pocket α, nearly spherical, which is almost entirely of $p_{x,y}$-character. At the G-point there is no hybridization between the $p_{x,y}$-orbital and d-orbital sets (I) and (II), as table 1 shows.

The electron-like Fermi surface β is dominated by the d_{xy}-orbital. It evolves tube-like along the G-Z-axis and only weakly hybridizes with other bands. The Fermi surface γ also almost spherically centred around the X-point is dominated by the p_z-orbital of cluster A hybridized with $d_{x^2-y^2}$-states of Ni. The Fermi surface δ has a flattened cylindrical topology and goes along the X–P–Q-direction and is contributed by all three orbitals from (I) and (II) sets. Finally, we find the Fermi surface pocket ε in the middle of octant dominated by p-orbitals.

3.3. Influence of antiferromagnetism on the Fermi surfaces

In the antiferromagnetically ordered phase the magnetic moments of the Dy-ion are ferromagnetically aligned within each plane and staggered along the z-axis with a magnetic wavevector $\boldsymbol{Q} = (0, 0, \pi/c)$. The position of the nearest-neighbour Dy-ions form a tetrahedron around the Ni-sites such that the four magnetic moments cancel each other. Thus the Ni-orbitals should not be spin polarized by the antiferromagnetic order. The spin polarization

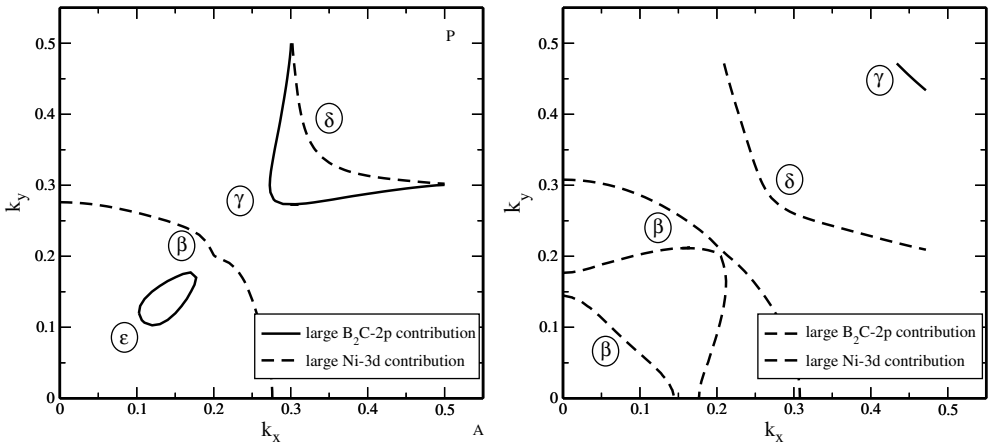

Figure 9. Cuts through the Brillouin zone perpendicular to [001] at $k_z = 0.16$ (left panel) and $k_z = 0.25$ (right panel).

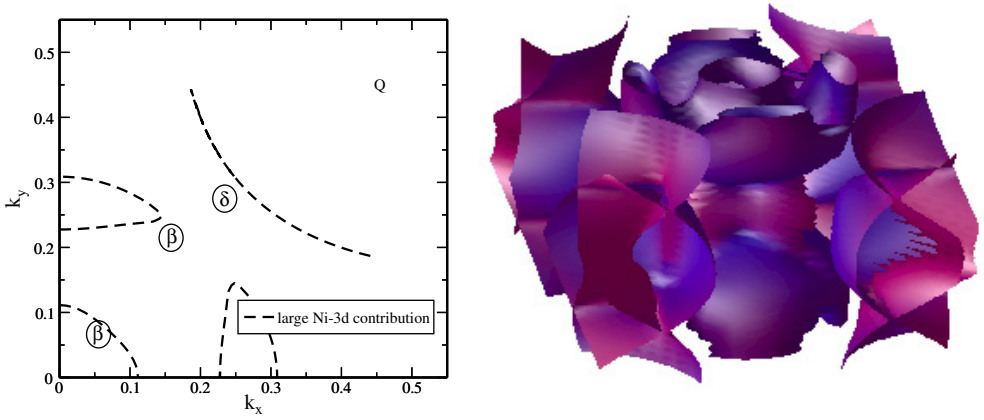

Figure 10. Cut through the Brillouin zone perpendicular to [001] at $k_z = 0.33$ (Z-point) (left panel). Right panel: three-dimensional Fermi surface. The degree of the light (red) and dark (blue) shade corresponds to the prevalence of the Ni-d and B–C–B-p states, respectively.

is transferred to the A 2p-orbitals. Thus, in order to visualize the influence of the magnetic order on the conduction electrons, we consider the admixture of A 2p-character to each Fermi surface. A band which has entirely Ni d_{xy}-character would not be affected by the ordered magnetic moments due to the canceling of the moments on the Ni-sites.

Apparently the Fermi surface β is almost exclusively of d_{xy} character and may be identified as the Fermi surface least affected by the antiferromagnetic order. On the other hand, the Fermi surfaces α, γ and ε have strong 2p-components and would be severely affected. It is also plausible to assume that they would play the leading role in mediating the RKKY-interaction for the realized magnetic order. In particular the α-sheet may be important for the ferromagnetic in-plane interaction while the G-sheet yields a leading wavevector not too far from $(0, 0, \pi/c)$ as our band structure calculation shows. However, the actual wavevector favoured by the γ-sheet $2k_{Fz}$ may be rather close to $\boldsymbol{Q}_{\rm inc} \approx 0.9\boldsymbol{Q}$ which appears as a fluctuation above $T_{\rm N}$ [7]. Naturally these two bands would fit into the scheme of de Gennes scaling, i.e. the mutual

influence of conduction electrons and localized spin is roughly following dG and depends on the magnitude of the magnetic moment. Also the ε-Fermi surface has a sizable 2p-contribution, while the δ-pocket is strongly dominated by the set (I) 3d-orbitals.

In the context of the phenomenological theory for the nucleation of superconductivity in the $Ho_{1-x}Dy_xNi_2B_2C$ in [1, 14] we may conclude that β and δ would constitute the Fermi surfaces for which the magnetic order is 'invisible'. Moreover the γ-pocket may be the leading among the other Fermi surfaces which remain normal in the magnetically ordered state but contribute to superconductivity in the paramagnetic phase. Our result suggests that the α- and γ-sheet (perhaps also ε) are never superconducting due to their strong coupling to the magnetic moment.

4. Conclusion

In the context of the phenomenological theory put forward in [1] the nickel–boron-carbide system appears as a multi-band superconductor [25, 26], where the magnetism influences different bands in different ways. The special structure of the antiferromagnetic order of the 4f magnetic moments suggests that a purely Ni 3d-based electronic band would not be affected by the magnetism due to geometric canceling on the Ni-sites. Our analysis of the LDA band structure of $DyNi_2B_2C$ reveals the existence of one such band which contains essentially only Ni 3d-orbital contribution at the Fermi surface and would provide a basis for superconductivity even in the magnetically ordered phase. The identified band has mainly Ni $3d_{xy}$ character and dominates the Fermi surfaces β and δ. On the other hand, there are several bands which involve strong 2p-components. They are unlikely to contribute to superconductivity in the magnetic phase, but may be important for the magnetic interactions.

If the cancelling of the magnetic moments is incomplete, due to fluctuations, then the moment is transferred to all bands. In this case also Hund's rule coupling becomes important, in particular, transferring the magnetic moments through the $3d_{x^2-y^2}$-orbitals which are strongly hybridized with the 2p-orbitals. They would carry the major contribution of the magnetic moments to the Ni-sites. We believe that our discussion in this paper gives a plausible and well-founded microscopic basis for the phenomenological approach to the unusual properties of the superconductivity in the alloy $Ho_{1-x}Dy_xNi_2B_2C$.

Acknowledgments

We would like to thank to H Doh, S I Lee, B K Cho for helpful discussions. This project was funded by the Swiss Nationalfonds and by NEDO of Japan. AOS and VIA are grateful to the Center for Theoretical Studies at ETH Zurich for support. This work was also supported by Russian Foundation for Basic Research under the grants RFFI-04-02-16096 and RFFI-03-02-39024, by Netherlands Organization for Scientific Research through NWO 047.016.005.

References

[1] Doh H *et al* 1999 *Phys. Rev. Lett.* **83** 5350
[2] Nagarajan R *et al* 1994 *Phys. Rev. Lett.* **72** 274
[3] Cava R J *et al* 1994 *Nature* **367** 146
[4] Cava R J *et al* 1994 *Nature* **367** 252
[5] Siegrist T *et al* 1994 *Nature* **367** 254
[6] Canfield P C *et al* 1998 *Phys. Today* **51** (10) 40
[7] Lynn J W *et al* 1998 *Phys. Rev.* B **55** 6584

[8] Cho B K *et al* 1996 *Phys. Rev. Lett.* **77** 163
[9] Thalmeier P and Zwicknagl G 2005 *Handbook on the Physics and Chemistry of Rare Earths* vol 34, ed K A Gschneidner Jr and LeRoy Eyring (Amsterdam: North Holland) p 135
[10] Nohara M *et al* 2000 *Physica* C **341–348** 2177
[11] Izawa K *et al* 2001 *Phys. Rev. Lett.* **86** 1327
[12] Boaknin E *et al* 2001 *Phys. Rev. Lett.* **87** 237001
[13] Maki K, Thalmeier P and Won H 2002 *Phys. Rev.* B **65** 140502
[14] Choi J-H *et al* 2001 *Phys. Rev.* B **65** 024520
[15] Siegrist T *et al* 1994 *J. Alloys Compounds* **216** 135
[16] Johansson B 1979 *Phys. Rev.* B **20** 1315
[17] Harrison W A 1984 *Phys. Rev.* B **29** 2917
[18] Singh D J 1991 *Phys. Rev.* B **44** 7451
[19] Anisimov V I *et al* 1991 *Phys. Rev.* B **43** 7570
[20] Andersen O K *et al* 1984 *Phys. Rev. Lett.* **53** 2571
[21] Andersen O K *et al* 1986 *Phys. Rev.* B **34** 5253
[22] Gunnarsson O *et al* 1989 *Phys. Rev.* B **39** 1708
[23] Pickett W E *et al* 1998 *Phys. Rev.* B **58** 1201
[24] Slater J C and Koster G F 1954 *Phys. Rev.* **94** 1498
[25] Shulga S V *et al* 1998 *Phys. Rev. Lett.* **80** 1730
[26] Drechsler S-L *et al* 1999 *Physica* C **317/318** 117